

## Neurite-based white matter alterations in *MAPT* mutation carriers: A multi-shell diffusion MRI study in the ALLFTD consortium

Nick Corriveau-Lecavalier<sup>a,b</sup>, Nirubol Tosakulwong<sup>c</sup>, Timothy G. Lesnick<sup>c</sup>, Angela J. Fought<sup>c</sup>, Robert I. Reid<sup>d</sup>, Christopher G. Schwarz<sup>d</sup>, Matthew L. Senjem<sup>d</sup>, Clifford R. Jack Jr.<sup>d</sup>, David T. Jones<sup>a,d</sup>, Prashanthi Vemuri<sup>d</sup>, Rosa Rademakers<sup>e,f</sup>, Eliana Marisa Ramos<sup>g</sup>, Daniel H. Geschwind<sup>h</sup>, David S. Knopman<sup>a</sup>, Hugo Botha<sup>a</sup>, Rodolfo Savica<sup>a</sup>, Jonathan Graff-Radford<sup>a</sup>, Vijay K. Ramanan<sup>a</sup>, Julie A. Fields<sup>b</sup>, Neill Graff-Radford<sup>i</sup>, Zbigniew Wszolek<sup>i</sup>, Leah K. Forsberg<sup>a</sup>, Ronald C. Petersen<sup>a</sup>, Hilary W. Heuer<sup>j</sup>, Adam L. Boxer<sup>j</sup>, Howard J. Rosen<sup>j</sup>, Bradley F. Boeve<sup>a</sup>, Kejal Kantarci<sup>d,\*</sup>, on behalf of the ALLFTD consortium

<sup>a</sup> Department of Neurology, Mayo Clinic, Rochester, MN, USA

<sup>b</sup> Department of Psychiatry and Psychology, Mayo Clinic, Rochester, MN, USA

<sup>c</sup> Department of Quantitative Health Sciences, Mayo Clinic, Rochester, MN, USA

<sup>d</sup> Department of Radiology, Mayo Clinic, Rochester, MN, USA

<sup>e</sup> Department of Neuroscience, Mayo Clinic Jacksonville, FL, USA

<sup>f</sup> Center for Molecular Neurology, Antwerp University, Belgium

<sup>g</sup> Department of Psychiatry, University of California San Diego, CA, USA

<sup>h</sup> Department of Neurology, University of California San Diego, CA, USA

<sup>i</sup> Department of Neurology, Mayo Clinic Jacksonville, FL, USA

<sup>j</sup> Department of Neurology, University of California San Francisco, CA, USA

### ARTICLE INFO

#### Keywords:

Frontotemporal dementia  
Diffusion magnetic resonance imaging  
Microtubule-associated protein tau  
Neurite orientation dispersion and density imaging  
Diffusion tensor imaging

### ABSTRACT

We assessed white matter (WM) integrity in *MAPT* mutation carriers (16 asymptomatic, 5 symptomatic) compared to 31 non-carrier family controls using diffusion tensor imaging (DTI) (fractional anisotropy; FA, mean diffusivity; MD) and neurite orientation dispersion and density imaging (NODDI) (neurite density index; NDI, orientation and dispersion index; ODI). Linear mixed-effects models accounting for age and family relatedness revealed alterations across DTI and NODDI metrics in all mutation carriers and in symptomatic carriers, with the most significant differences involving fronto-temporal WM tracts. Asymptomatic carriers showed higher entorhinal MD and lower cingulum FA and patterns of higher ODI mostly involving temporal areas and long association and projections fibers. Regression models between estimated time to or time from disease and DTI and NODDI metrics in key regions (amygdala, cingulum, entorhinal, inferior temporal, uncinate fasciculus) in all carriers showed increasing abnormalities with estimated time to or time from disease onset, with FA and NDI showing the strongest relationships. Neurite-based metrics, particularly ODI, appear to be particularly sensitive to early WM involvement in asymptomatic carriers.

**Abbreviations:** ALLFTD, ARTFL LEFTDS Longitudinal Frontotemporal Lobar Degeneration; bvFTD, Behavioral variant frontotemporal dementia; CDR plus NACC FTLD-SB, Clinical Dementia Staging Instrument plus NACC FTLD Behavior and Language Domains sum of boxes; CI, Confidence intervals; dMRI, Diffusion magnetic resonance imaging; DTI, Diffusion tensor imaging; EPI, Echo planar imaging; f-FTLD, Familial frontotemporal lobar degeneration; FA, Fractional Anisotropy; FDR, False Discovery Rate; ISOVF, Isotropic Value Fraction; MRI, Magnetic resonance imaging; MPRAGE, Magnetization-prepared rapid gradient echo; *MAPT*, Microtubule-associated protein tau; MD, Mean diffusivity; MBI, Mild behavioral impairment; MoCA, Montreal Cognitive Assessment; NODDI, Neurite Orientation Dispersion and Density Imaging; NDI, Neurite density index; tNDI, Tissue-weighted Neurite Density Index; ODI, Orientation and dispersion index; ROI, Region of interest; WM, White matter.

\* Correspondence to: Mayo Clinic, 200 First Street S.W., Rochester, MN 55905, USA.

E-mail address: [kantarci.kejal@mayo.edu](mailto:kantarci.kejal@mayo.edu) (K. Kantarci).

<https://doi.org/10.1016/j.neurobiolaging.2023.12.001>

Received 5 July 2023; Received in revised form 28 November 2023; Accepted 1 December 2023

Available online 10 December 2023

0197-4580/© 2023 The Authors. Published by Elsevier Inc. This is an open access article under the CC BY-NC license (<http://creativecommons.org/licenses/by-nc/4.0/>).

## 1. Introduction

Mutations on the microtubule associated protein tau (*MAPT*) gene cause around 5–20% of familial frontotemporal lobar degeneration (f-FTLD) (Moore et al., 2020; Ramos et al., 2020; Sieben et al., 2012). These mutations are most often associated with early-onset clinical syndromes predominantly involving behavior and personality, in addition to other syndromes primarily targeting memory, language, and/or motor functions, although to a lesser prevalence (Boeve et al., 2022). Several efforts have been undertaken to characterize brain abnormalities in *MAPT* mutation carriers using magnetic resonance imaging (MRI) and/or diffusion MRI (dMRI) (Chen and Kantarci, 2020; Peet et al., 2021). One consistent finding is the selective atrophy of gray matter in the medial temporal lobe (Cash et al., 2018; Chu et al., 2021; Fumagalli et al., 2018; Staffaroni et al., 2022) and the degeneration of regional frontotemporal white matter (WM) tracts and long association and projection fibers connecting these primarily affected areas to the rest of the brain (Chen et al., 2019; Chu et al., 2021). Importantly, a growing number of investigations have found that WM abnormalities are observable in asymptomatic *MAPT* mutation carriers compared to family non-carriers several years prior to the onset of clinical symptoms (Chen et al., 2019; Dopper et al., 2014; Jiskoot et al., 2018). These abnormalities mostly involve changes in mean diffusivity (MD) and fractional anisotropy (FA) in tracts known to be implicated in *MAPT* mutations, notably the uncinate fasciculus (Chen et al., 2019; Dopper et al., 2014; Jiskoot et al., 2018) and the cingulum (Jiskoot et al., 2018). Moreover, one longitudinal study from our group has shown an increase of entorhinal MD in asymptomatic *MAPT* mutation carriers, and these changes correlated with estimated time to symptom onset (Chen et al., 2019). These findings position WM alterations as an important candidate to shed light on the earliest pathognomonic processes associated with *MAPT* mutations and estimate where an individual stands along the pathobiological spectrum of the disease.

Recent technological advances in the area of dMRI have made Neurite Orientation Dispersion and Density Imaging (NODDI) (Edwards et al., 2017; Zhang et al., 2012) feasible for multi-site study with cognitively impaired participants. NODDI is a multi-shell model that can measure biological properties related to WM integrity. It is divided into three properties: Neurite Density Index (NDI), which represents the fraction of restricted (tissue) water contained within neurites (thin pipes, i.e., axons), the volume fraction of unrestricted (and as a consequence, isotropically diffusing) with free water (isotropic value fraction or ISOVF), and Orientation Dispersion Index (ODI), which represents the extent to which the neurite directions are dispersed. NODDI measures differ from traditional diffusion tensor imaging (DTI) products (FA and MD) in that by explicitly modeling the intra-axonal (neurite), extracellular (but within tissue) and CSF components, they separate effects such as axonal degeneration, changes in axonal arrangement (dispersion), and overall atrophy (encroachment by CSF). In contrast, MD and FA look at the overall diffusivity and anisotropy of the whole voxel without discerning the fractions of different water environments inside the voxel (Soares et al., 2013; Thomason and Thompson, 2011). Thus, NODDI is meant to offer results that are interpretable in terms of biophysical parameters of brain tissue.

While NODDI has not been extensively applied as DTI in neurodegenerative diseases, recent evidence has shown that NODDI metrics provide greater sensitivity than FA and MD to tau pathology in mice models of Alzheimer's disease (Colgan et al., 2016) and to WM alterations in amyotrophic lateral sclerosis (Barritt et al., 2018), and could identify patterns of imaging abnormalities specific to cerebrovascular disease, tauopathies and TDP-43 pathology in humans (Raghavan et al., 2022). Therefore, NODDI may have the potential to capture the earliest WM changes associated with neurodegenerative processes, although it has not been applied in f-FTLD and more specifically in *MAPT* mutation carriers. This endeavor is particularly important given the rarity of *MAPT* mutation carriers in the general population, which underscores

the need for sensitive biomarkers to enrich clinical trials.

We aimed to assess axonal integrity in *MAPT* mutation carriers and early WM neurodegeneration in asymptomatic carriers using traditional DTI (FA and MD) and NODDI measurements (NDI and ODI). To this end, we obtained data from asymptomatic and symptomatic *MAPT* mutation carriers and family non-carriers with available multi-shell dMRI from the ARTFL/LEFTDS Longitudinal Frontotemporal Lobar Degeneration (ALLFTD) cohort. We first compared DTI and NODDI metrics between *MAPT* carriers and family non-carriers across a wide set of regions of interest (ROIs) to determine which areas best discriminate these groups. This was done in all *MAPT* carriers versus family controls, and then in asymptomatic and symptomatic *MAPT* carriers versus controls. We then performed a secondary analysis with DTI and NODDI values in a few key brain regions identified based on the initial analysis on group differences and determined associations between these metrics and actual time of (for symptomatic carriers) or estimated time to (for asymptomatic carriers) symptom onset in all *MAPT* mutation carriers.

## 2. Methods

### 2.1. Participants

In the context of this study, we included demographic, clinical, and genetic results from participants with a confirmed *MAPT* genetic mutation and non-carrier first-degree relatives who had available multi-shell dMRI data from the ALLFTD cohort from June 2020 to November 2021. This resulted in 52 participants from 4 ALLFTD sites, of which 21 carried a *MAPT* mutation and 31 were non-carrier relatives which were included as controls. Among *MAPT* mutation carriers, 5 were in the symptomatic phase of the disease (see details below) and 16 were asymptomatic. Scanning sites included were MGH/Harvard (n = 6, 12%), Washington University (St. Louis) (n = 2, 4%), Mayo Clinic Jacksonville (n = 7, 13%) and Mayo Clinic Rochester (n = 37, 71%).

Clinical diagnoses were attributed by clinicians experienced in FTD and were based on medical history review, mental status examination, and a neurological examination. Mental status examination was done using the Montreal Cognitive Assessment (MoCA) (Nasreddine et al., 2005) and the Clinical Dementia Staging Instrument plus NACC FTLD Behavior and Language Domains sum of boxes (CDR plus NACC FTLD-SB) (Knopman et al., 2008). Of the five symptomatic carriers, three were diagnosed with bvFTD (Rascovsky et al., 2011), one had mild behavioral and/or cognitive impairment (MBCI) (Barker et al., 2022) and one was diagnosed with an Alzheimer's disease-like amnesic syndrome (McKhann et al., 2011).

Inclusion criteria for this specific study were: 1) being a member of a family with a known *MAPT* mutation and at an age of 18 years or older; 2) the predominant phenotype in the kindred should be in either the behavioral/cognitive domain and not motor (i.e., parkinsonism or amyotrophic lateral sclerosis), 3) presence of a reliable informant who is in contact with the participant on a weekly basis, 4) being sufficiently fluent in English to complete all measures, 5) being willing and able to consent to the protocol and undergo yearly assessments, 6) being willing to undergo neuropsychological assessments, and 7) not having contraindications for MRI examination. Exclusion criteria were: 1) absence of a known *MAPT* mutation in the participant or the family, 2) presence of a structural brain lesion (e.g., tumor, stroke), and 3) presence of a neurological condition that could alter findings (e.g., clinical diagnosis of multiple sclerosis).

### 2.2. Standard protocols approvals, registrations, and patient consents

The ALLFTD study was approved by the Trial Innovation Network at Johns Hopkins University, and local ethics committees at each of the sites approved the study. All participants or their legally authorized representatives provided written and informed consent to take part in the study.

### 2.3. Genetic testing

All participants underwent genetic screening at the University of California, Los Angeles using published methods (Ramos et al., 2020). Briefly, DNA samples were screened using targeted sequencing of a custom panel of genes previously demonstrated to be implicated in frontotemporal lobar degeneration, including *MAPT* and progranulin (*GRN*). The presence of hexanucleotide repeat expansions in *C9orf72* was assessed using both fluorescent and repeat-primed PCR. Participants with a *GRN* mutation or an *C9orf72* expansion were not considered for this study.

### 2.4. Image acquisition and processing

The MRI sequences used in this analysis included T<sub>1</sub>-weighted and multi-shell diffusion weighted scans. They were performed on four 3 T Siemens Prisma scanners (Siemens Healthcare, Erlangen, Germany) at four different sites. The T<sub>1</sub>-weighted scans used a 3D magnetization-prepared rapid gradient echo (MPRAGE) sequence with repetition time 2300 ms, echo time 3.14 ms, and inversion time 945 ms, flip angle 9°, and 1.0 mm isotropic resolution. The diffusion weighted images were acquired with a spin echo single shot Echo Planar Imaging (EPI) sequence with 2.0 mm isotropic voxels. The echo times varied with scanner model from 62 to 93 ms, with the majority having 71 ms. Each scan had 13 b = 0, 6 b = 500, 48 b = 1000, and 60 b = 2000 s/mm<sup>2</sup> volumes, with the diffusion gradients in each shell evenly spread using an electrostatic repulsion scheme (Caruyer et al., 2013), modified to distribute them over whole spheres instead of hemispheres.

After denoising (Veraart et al., 2016) the diffusion weighted images, head motion and eddy current distortion were corrected using FSL's eddy program (Andersson et al., 2016, 2017; Andersson and Sotiropoulos, 2016). We corrected for Gibbs ringing (Kellner et al., 2016) and then skull stripped the images (Reid et al., 2018). The Rician noise bias was then removed (Koay et al., 2009). The reason we run “unring” after “eddy” is that although most of the ringing is intrinsic to the acquisition, some is also added by eddy when it interpolates the image because of fractional voxel motions and eddy current distortions. It uses a higher order (than linear) interpolation, which achieves less blurring at the cost of some ringing. Running unring after eddy is done to correct ringing from both the acquisition and eddy. Diffusion tensors were estimated using nonlinear least squares fitting and used to calculate FA and MD images (Garyfallidis et al., 2014). ANTS (Avants et al., 2014) was used to nonlinearly register a modified version of the JHU “Eve” WM atlas (Oishi et al., 2009) to each subject's FA image. Voxels with MD > 2 x 10<sup>-3</sup> or < 7 x 10<sup>-5</sup> mm<sup>2</sup>/s were excluded as mostly CSF or air, respectively, and the median FA and MD were calculated in each ROI. The cuneus, precuneus, fusiform, and lingual WM regions were excluded since they were too small for reliable registration. Although echo-planar imaging distortion was not explicitly corrected for, it was implicitly corrected for since the findings were from nonlinearly warping the JHU “Eve” FA image to each subject's FA image. The atlas registrations were then inspected for quality control by an image analyst (RR).

For each region (except the pons, medulla, and midbrain, for susceptibility and coverage issues), we then estimated the DTI and NODDI values as the median of the voxel values within the ROI. The median was used to minimize any possible influence from artifacts or partial volume contamination at ROI boundaries. We also converted NDI, the fraction of tissue that is neurites, into tissue-weighted NDI, a quantity proportional to the total number of neurites in each voxel, as tNDI = NDI \* (1 - ISOVF). All DTI and NODDI metrics were combined across hemispheres. This was done because it is well established that patterns of brain abnormalities in *MAPT* mutation carriers show symmetrical patterns across hemispheres (Fumagalli et al., 2018; Rohrer et al., 2010; Whitwell et al., 2009).

### 2.5. Statistical analyses

Demographic and clinical data were compared between asymptomatic *MAPT* mutation carriers, symptomatic *MAPT* mutation carriers and family controls using generalized linear mixed models and linear mixed models for categorical and continuous variables, respectively. These models were adjusted for age and accounted for the family structure using random effects. Tukey contrasts were subsequently used for pairwise comparisons when the omnibus test was significant.

Weighted median values for FA, MD, tNDI and ODI for each region of the JHU atlas were log-transformed. Between-site data were harmonized using ComBat, a batch-effect correction tool which has been shown to preserve biological variability due to covariates of interest (i.e., age and diagnosis) while removing unwanted variation introduced by site in dMRI data (Fortin et al., 2017). Mixed effect linear models were used to assess WM alterations in *MAPT* mutation carriers. This type of model is an extension of simple linear models that allows to account for non-independence in the data. This is particularly relevant to this study given that a substantial proportion of *MAPT* mutation carriers were recruited along with non-carriers from the same family. Separate models were fit across all regions for each measure (FA, MD, tNDI, ODI) in all *MAPT* mutation carriers versus controls, then in asymptomatic and symptomatic *MAPT* mutation carriers versus controls. Age was centered at 45 (mean age of all participants). Family relatedness was included in each mixed model as a random family-specific intercept effect. A false discovery rate (FDR) correction for multiple comparisons was applied across all ROIs, and within each dMRI measure.

We then performed a follow-up analysis to determine which dMRI metric was able to best distinguish between all *MAPT* mutation carriers versus non-carriers based on group-wise comparisons results. We combined the median values of each significant ROI per metric into a “meta-ROI” weighted for the number of voxels in each ROI, thus resulting in four meta-ROIs (FA, MD, tNDI and ODI) for each patient. We then used mixed effect linear models as described above to compare all *MAPT* mutation carriers versus non-carriers on these meta-ROIs and compared models by assessing the overlap in estimate confidence intervals (CIs).

We conducted secondary analyses to assess the association of estimated time until (for asymptomatic carriers) or time since (for symptomatic carriers) disease onset and DTI and NODDI metrics in a set of key ROIs which were determined based on the results of group-wise comparisons described above. Given that time to symptom onset was not available in asymptomatic carriers, we calculated the estimated time to symptom onset according to the age at symptom onset in the symptomatic carrier from the kindred. It is thus possible that some asymptomatic carriers may be past their estimated age at symptom onset, due to the variability across *MAPT* mutations and even within families with the same *MAPT* mutation in terms of age at symptom onset (Domoto-Reilly et al., 2017; Manoochehri et al., 2023). We then fit linear regression models between each log-transformed DTI and NODDI metric and actual/estimated time to symptom onset across all *MAPT* mutation carriers. We conducted sensitivity analyses using Cook's distance to assess whether significant change in slopes could be caused by influential observations, where an observation with a value greater than 0.5 was considered influential.

## 3. Results

### 3.1. Demographic and clinical data

Demographic and clinical data, along with group-wise comparisons results, are displayed in Table 1. On average, asymptomatic carriers were younger than both symptomatic carriers and family controls. As expected, symptomatic carriers had lower MoCA and higher FTLD CDR SOB scores compared to asymptomatic carriers and family controls. There were no other significant differences. Due to the relatively small number of *MAPT* mutation carriers in this analysis and potential risk to

**Table 1**  
Demographic and clinical data.

	Asymptomatic	Symptomatic	Non-carrier	P-value
Sample size	16	5	31	-
Age at visit (years)	36 [26,44]	54 [50,58]	48 [34,60]	0.01*
Female, n (%)	13 (81%)	4 (80%)	17 (55%)	0.10
Education (years)	14 [13,16]	18 [16,20]	16 [14,18]	0.17
FTLD-CDR SOB	0.0 [0.0, 0.0]	6.7 [5.0, 7.5]	0.0 [0.0, 0.0]	< 0.001 <sup>†</sup>
MoCA	28 [26,29]	22 [20,25]	27 [27,29]	0.002 <sup>‡</sup>

Data are expressed as mean with interquartile range in brackets. \*Asymptomatic < non-carrier ( $P = 0.03$ ), and symptomatic ( $P = 0.02$ ); <sup>†</sup>Symptomatic > non-carrier, and asymptomatic ( $P < 0.001$ ); <sup>‡</sup>Symptomatic < non-carrier ( $P < 0.001$ ), and asymptomatic ( $P = 0.003$ ). FTLD-CDR SOB = Frontotemporal lobar degeneration clinical dementia rating sum of boxes; MoCA = Montreal cognitive assessment.

maintaining confidentiality if specific mutations were stated, the information on specific mutations is purposefully not included in this report.

### 3.2. Models in all MAPT carriers versus controls

Complete statistical results of linear mixed-effects models can be

found in [Supplementary Tables 1 and 2](#), along with forest plots displayed on [Supplementary Figures 1 and 2](#). Brain renderings of these results are shown in [Figs. 1 and 2](#).

When considering traditional DTI metrics, lower FA values were found in all *MAPT* mutation carriers compared to controls, including the inferior temporal and entorhinal regions and the cingulum, and these differences remained after correcting for multiple comparisons. Additional areas were also found to have lower FA values in *MAPT* mutation carriers, although they were not significant after correcting for multiple comparisons, and those include the superior occipital, gyrus rectus, superior and medial temporal WM regions, the hippocampal portion of the cingulum and long association and projecting fibers involving the external capsule, and the uncinate, inferior and lateral fronto-occipital fasciculi. Higher MD values were found in *MAPT* mutation carriers compared to controls, including the entorhinal WM and amygdala, and these differences remained after applying corrections for multiple comparisons. Additional areas with higher MD values were found in *MAPT* mutation carriers that were no longer significant after correcting for multiple comparisons, which involve the superior frontal, middle and lateral orbito-frontal, inferior temporal, hippocampal and gyrus rectus WM, the inferior fronto-occipital and uncinate fasciculi and the genu of the corpus callosum.

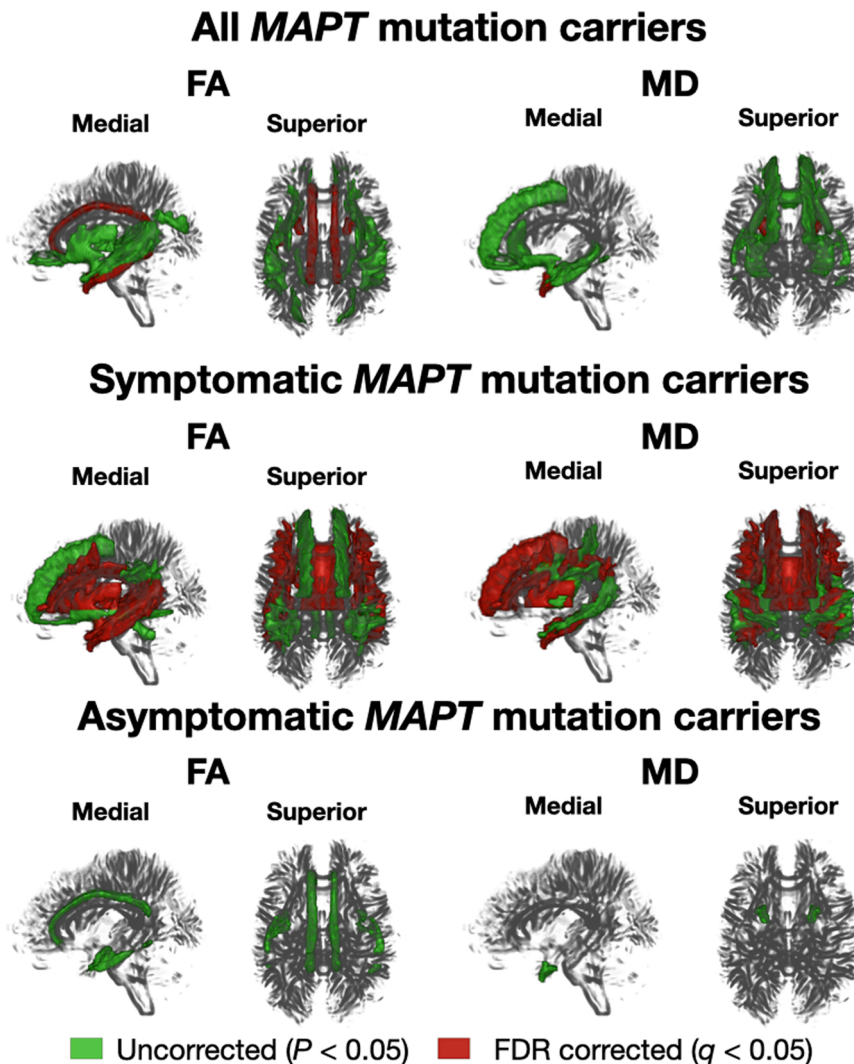


**Fig. 1.** Region of interest analyses. Green areas are statistically significant at an uncorrected threshold of  $P < 0.05$ , while red areas are statistically significant after applying a false discovery rate correction for multiple comparisons at a threshold of  $q < 0.05$ . Of note, these differences reflect lower FA values and higher MD values in *MAPT* carriers compared to controls. FA = Fractional anisotropy; MD = Mean diffusivity. MRicroGL (<http://www.mccauslandcenter.sc.edu/mricrogl/>) was used to display the results.

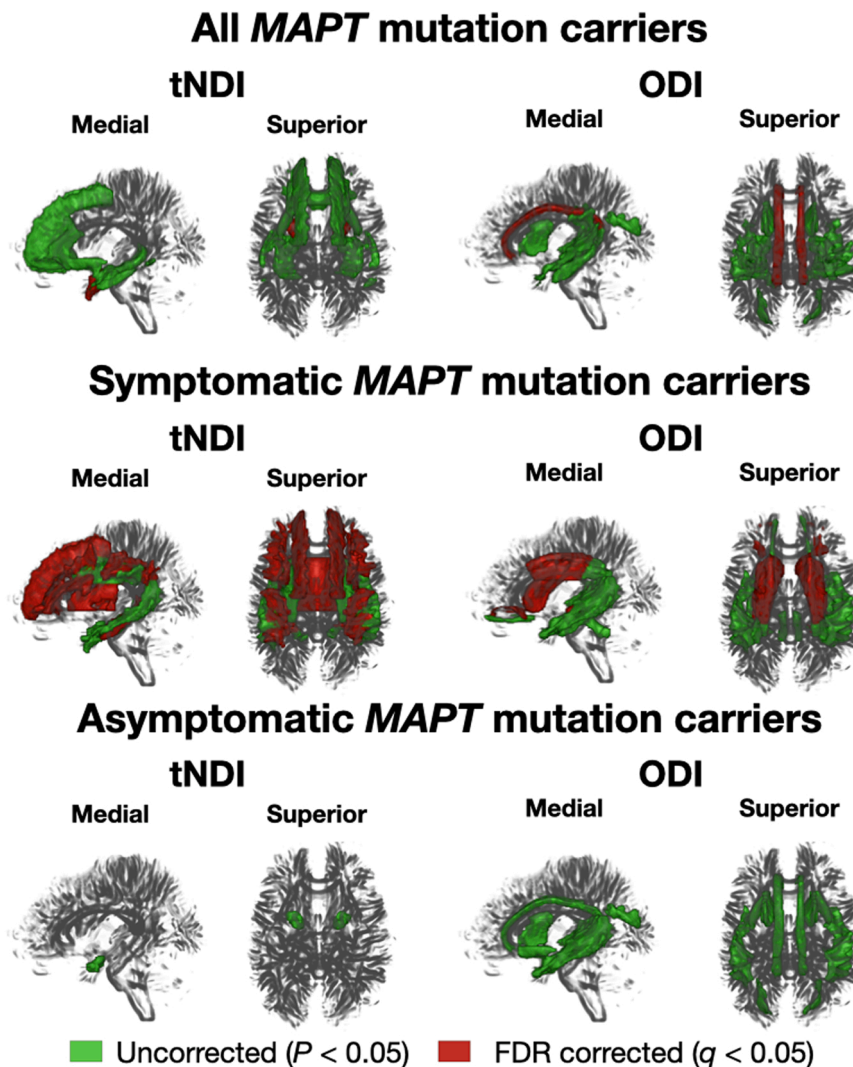


**Fig. 2.** Region of interest analyses. Green areas are statistically significant at an uncorrected threshold of  $P < 0.05$ , while red areas are statistically significant after applying a false discovery rate correction for multiple comparisons at a threshold of  $q < 0.05$ . Of note, these differences reflect lower tNDI values and higher ODI values in *MAPT* carriers compared to controls. tNDI = tissue-weighted Neurite Density Index; ODI = Orientation Dispersion Index. MRICROGL (<http://www.mccauslandcenter.sc.edu/mricrogl/>) was used to display the results.

When considering NODDI metrics, models revealed lower tNDI values in *MAPT* mutation carriers relative to controls in the entorhinal WM and amygdala, and these differences remained after applying corrections for multiple comparisons. Other areas showed lower tNDI values in *MAPT* carriers, although not surviving multiple comparisons, including focal areas such as the lateral fronto-orbital, superior frontal, inferior temporal, gyrus rectus and hippocampal regions, and long association fibers including the uncinate and inferior fronto-occipital fasciculi, the genu of the corpus callosum and the anterior portion of the corona radiata. Higher ODI values were observed in *MAPT* mutation carriers relative to controls and were found in the cingulum, and only this area remained after including corrections for multiple comparisons. Additional areas with higher ODI values in *MAPT* carriers without surviving multiple comparisons correction include the hippocampus, superior temporal, superior occipital and supramarginal WM, the superior fronto-occipital fasciculus, the hippocampal portion of the cingulum, the fornix stria terminalis, and the anterior limb of the internal capsule.

### 3.3. Models in symptomatic and asymptomatic *MAPT* carriers versus controls

Below we describe results from the mixed-effect linear models

comparing symptomatic *MAPT* carriers and asymptomatic *MAPT* carriers to controls for each DTI metric. Even though all three groups were included in these models, we will first describe results in symptomatic carriers versus controls, followed by asymptomatic carriers versus controls.

### 3.4. Results in symptomatic *MAPT* carriers versus controls

When considering traditional DTI metrics, lower FA values were found in symptomatic *MAPT* carriers relative to controls in several WM regions and tracts including the entorhinal, inferior, superior and middle temporal, inferior and middle frontal WM, as well as long association and projecting fibers involving the fornix and fornix stria terminalis, body and genu of corpus callosum, the external capsule, and the uncinate fasciculus, and these differences remained after applying corrections for multiple comparisons. Additional areas showed lower FA values in symptomatic *MAPT* carriers relative to controls, but these differences did not remain after correcting for multiple comparisons including the middle fronto-orbital, superior frontal and supramarginal WM, as well as long association and projection fibers including the posterior corona radiata, superior cerebellar peduncle, sagittal stratum and inferior fronto-occipital fasciculus. Higher MD values were found in

symptomatic *MAPT* carriers relative to controls in the amygdala and hippocampus, entorhinal, angular, inferior, middle and superior frontal WM and long association and projecting fibers involving the body of the corpus callosum, fornix, external capsule, and superior longitudinal fasciculus, and these differences remained after correcting for multiple comparisons. Other areas with higher MD values in symptomatic *MAPT* carriers relative to controls that did not remain statistically significant after correcting for multiple comparisons involved the supramarginal, middle temporal, post-central WM, the globus pallidum, the hippocampal portion of the cingulum, the posterior limb of the internal capsule and the superior corona radiata.

When considering NODDI metrics, lower NDI values were found in symptomatic *MAPT* mutation carriers relative to controls in regions of hippocampus, angular, and inferior, middle and superior frontal WM as long association and projecting fibers including the body of the corpus callosum, external capsule, fornix, and superior longitudinal fasciculus, and these differences remained statistically significant after correcting for multiple comparisons. Additional regions with lower NDI values in symptomatic *MAPT* carriers that did not remain statistically significant after correcting for multiple comparisons included the amygdala, entorhinal, middle temporal, supramarginal WM as well as the hippocampal portion of the cingulum and the superior corona radiata. Higher ODI values were found in symptomatic *MAPT* mutation carriers relative to controls in the lateral orbito-frontal WM, caudate, fornix stria terminalis and superior corona radiata, and these differences remained statistically significant after correcting for multiple comparisons. Other regions, such as the hippocampus, middle and superior temporal and middle fronto-orbital WM as well as the posterior corona radiata and superior cerebellar peduncles, had higher ODI values in symptomatic *MAPT* carriers, but these differences did not remain statistically significant after correcting for multiple comparisons.

### 3.5. Results in asymptomatic *MAPT* carriers versus controls

When considering traditional DTI metrics, lower FA values were found in the cingulum and the inferior temporal WM and higher MD was found in the entorhinal WM in asymptomatic *MAPT* mutation carriers relative to controls. None of these differences remained statistically significant after correcting for multiple comparisons.

When considering NODDI metrics, lower tNDI values were observed in asymptomatic *MAPT* mutation carriers relative to controls in the amygdala, but this difference did not remain after correcting for multiple comparisons. A widespread pattern of higher ODI values was found in asymptomatic *MAPT* mutation carriers relative to controls, which involved the middle and superior temporal and superior occipital WM as well as long association and projection fibers including the superior and inferior fronto-occipital fasciculi, the cingulum, and the anterior limb of the internal capsule, although none of these differences remained statistically significant after correcting for multiple comparisons.

### 3.6. Assessment of meta-ROIs to distinguish between all *MAPT* carriers versus controls

Comparisons of values in meta-ROIs incorporating significant regions for each metric revealed significant differences between all *MAPT* carriers compared to controls for all models, as expected. Comparisons between models (while flipping signs for tNDI and FAs) revealed that the tNDI meta-ROI model (estimate: 0.136, CIs: 0.072–0.199) outperformed the FA meta-ROI model (estimate: 0.044, CIs: 0.019–0.069) as supported by non-overlapping CIs. Models for MD (estimate: 0.119, CIs: 0.062–0.177) and ODI (estimate: 0.112, CIs: 0.060–0.163) meta-ROIs did not significantly differ from models for FA and tNDI.

### 3.7. Modelling of DTI and NODDI metrics in relation to actual/estimated time to symptom onset

The associations between DTI and NODDI metrics and time to actual/estimated time to symptom onset was assessed in key ROIs. The selection of these ROIs was based on the results from the between-group comparisons, where we selected those ROIs showing statistically significant findings across most metrics in *MAPT* mutation carriers relative to controls. This included the amygdala, cingulum, entorhinal, inferior temporal, and uncinate fasciculus WM regions. Of note, FA was not included for the amygdala given that this is a gray matter area. Results for the regression models between actual/estimated time to symptom onset and DTI and NODDI metrics can be found in Table 2 and scatterplots demonstrating these relationships are displayed in Figs. 3 and 4. Sensitivity analyses identified an influential observation (asymptomatic carrier) across several associations. When the influential observation was excluded, qualitative changes in statistical significance were always

**Table 2**  
Regression models between diffusion metrics and age at actual/estimated symptom onset.

Metric	Region	All participants		Removing one outlier	
		Estimates (95% CI)	P-value	Estimates (95% CI)	P-value
FA	Cingulum	-0.003 (-0.005, -0.002)	< 0.001	No outlier	
	Entorhinal	-0.007 (-0.01, -0.001)	0.02	-0.01 (-0.02, -0.005)	0.002
	Inferior temporal	-0.003 (-0.006, -0.001)	0.002	No outlier	
	Uncinate fasciculus	-0.003 (-0.006, -0.000)	0.04	-0.005 (-0.008, -0.002)	0.004
MD	Amygdala	0.006 (-0.001, 0.01)	0.08	0.01 (0.002, 0.02)	0.02
	Cingulum	0.000 (0.000, 0.002)	0.04	No outlier	
	Entorhinal	0.005 (0.000, 0.01)	0.04	0.008 (0.003, 0.01)	0.007
	Inferior temporal	0.002 (0.000, 0.004)	0.048	0.003 (0.001, 0.005)	0.02
tNDI	Uncinate fasciculus	0.000 (-0.000, 0.002)	0.13	No outlier	
	Amygdala	-0.006 (-0.01, 0.001)	0.09	-0.01 (-0.02, -0.002)	0.02
	Cingulum	-0.002 (-0.003, -0.001)	0.005	No outlier	
	Entorhinal	-0.006 (-0.01, 0.001)	0.09	-0.01 (-0.02, -0.002)	0.02
ODI	Inferior temporal	-0.003 (-0.005, -0.000)	0.046	No outlier	
	Uncinate fasciculus	-0.001 (-0.003, 0.000)	0.10	-0.002 (-0.004, -0.000)	0.03
	Amygdala	-0.001 (-0.005, 0.003)	0.60	No outlier	
	Cingulum	0.006 (0.001, 0.01)	0.02	No outlier	
ODI	Entorhinal	0.002 (-0.001, 0.005)	0.17	No outlier	
	Inferior temporal	0.000 (-0.004, 0.006)	0.71	-0.001 (-0.008, 0.005)	0.63
	Uncinate fasciculus	0.001 (-0.003, 0.005)	0.56	0.004 (0.000, 0.009)	0.04

DTI = Diffusion Tensor Imaging; CI = Confidence intervals; FA = Fractional anisotropy; MD = Mean diffusivity; tNDI = tissue-weighted Neurite Density Index; ODI = Orientation and Dispersion Index.

### Fractional anisotropy and mean diffusivity

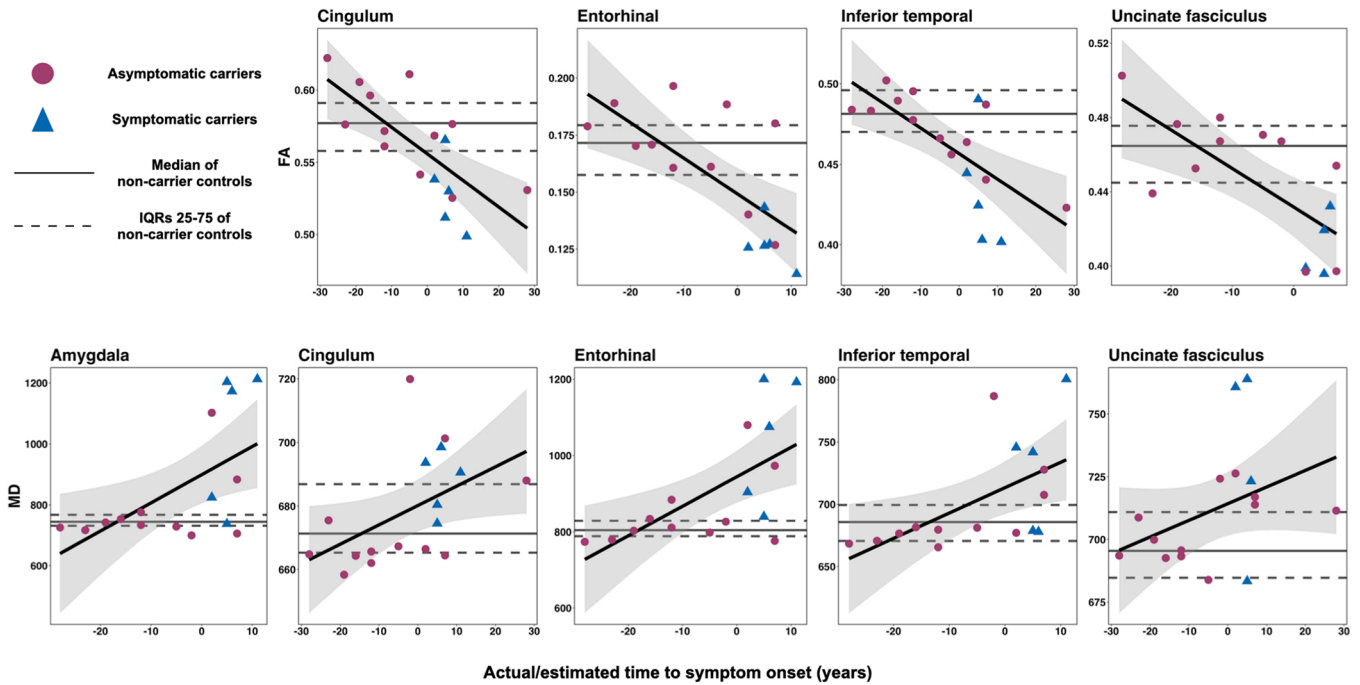


Fig. 3. Regression models between actual/estimated time to symptom onset and FA and MD. Only models excluding the influential observation are displayed. FA = Fractional anisotropy; MD = Mean diffusivity; IQR = Interquartile range.

### Tissue-weighted neurite density index and orientation and dispersion index

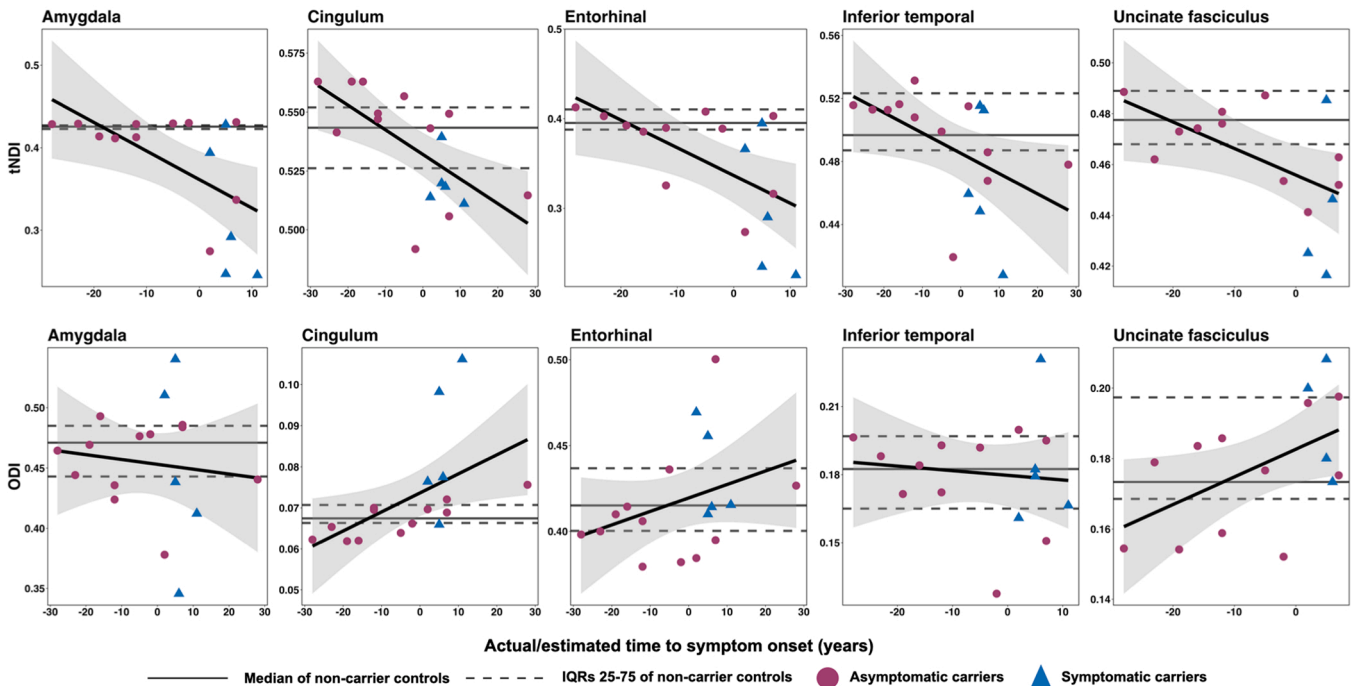


Fig. 4. Regression models between actual/estimated time to symptom onset and NODDI DTI metrics. tNDI = tissue-weighted Neurite Density Index; ODI = Orientation Dispersion Index; IQR = Interquartile Range.

in the direction of finding statistical significance without the influential observation.

Considering FA, models were statistically significant across all ROIs and showed negative relationships, with and without excluding the

influential observation. This means that lower FA values were observed with more advanced estimated/actual disease progression. Models for MD showed significant and positive relationships in the cingulum, entorhinal and inferior temporal areas, with and without excluding the

influential observation. This means that higher MD values related with more advanced estimated/actual disease progression in these regions. Models in the amygdala showed similar relationships, although only the model excluding the influential observation was significant. There was no significant relationship for MD in the uncinata fasciculus.

Models for tNDI showed significant and negative relationships in the cingulum and the inferior temporal regions, lower values related with more advanced estimated/actual disease progression. Models in the amygdala, the entorhinal and uncinata fasciculus regions showed similar relationships, although only models excluding the influential observation were significant. Models for ODI showed significant and positive relationships for the cingulum, meaning that higher values were associated with more advanced estimated/actual disease progression. A similar relationship was found in the uncinata fasciculus, although only the model excluding the influential observation was significant. Other models for ODI were not significant.

#### 4. Discussion

We used traditional DTI and recently developed NODDI metrics to assess WM integrity in *MAPT* mutation carriers and early axonal abnormalities in asymptomatic carriers. Models in all *MAPT* mutation carriers revealed overlapping patterns across different dMRI metrics mostly involving regional frontotemporal areas and projecting tracts and long associations fibers connecting these areas to the rest of the brain. Similar widespread WM abnormality patterns were found in symptomatic carriers. In symptomatic carriers, however, traditional DTI metrics revealed patterns of WM alterations restricted to the medial temporal lobe, whereas widespread patterns of increased axonal dispersion (i.e., ODI) were observed. Additionally, a follow-up, exploratory analysis showed that the combination of differences observed for tNDI outperformed FA in distinguishing *MAPT* carriers from controls. Our results suggest that DTI and NODDI measurements may have different sensitivities to WM alterations in *MAPT* mutation carriers. Importantly, measurements that separated axon-type water from other compartments, particularly ODI, were sensitive to early WM abnormalities during the asymptomatic phase of the disease. In a secondary analysis, we demonstrated that dMRI measures, especially FA and tNDI, track with disease progression in time and therefore may potentially be used in predicting time to phenocconversion.

dMRI studies that have examined tau-mediated WM injury have generally reported reduced FA and increased MD in areas known to be vulnerable to large-scale degeneration in *MAPT* mutation carriers, including frontotemporal areas and structurally connected tracts such as the uncinata fasciculus and the cingulum (Chen and Kantarci, 2020; Jiskoot et al., 2018, 2019; Panman et al., 2019). Thus, our findings with FA and MD are in agreement with previous studies. It is also worth noting that higher MD was found in the entorhinal WM only in asymptomatic carriers, and that this metric also tracked with actual or estimated age at symptom onset across all *MAPT* carriers. This is highly consistent with findings from Chen et al. (Chen et al., 2019), where longitudinal increase in entorhinal MD was also found to distinguish asymptomatic *MAPT* mutation carriers from family controls and to track with estimated disease progression. However, this study failed to find significant differences in FA values in asymptomatic carriers, whereas we found lower FA in the cingulum and inferior temporal WM. This may be due to the inclusion of a larger number of asymptomatic carriers in our study. Overall, our results in FA and MD appear to faithfully replicate previous findings, further consolidating the reliability of traditional DTI to measure WM abnormalities in *MAPT* carriers.

The novel aspect of this study is the inclusion of NODDI to assess WM abnormalities in *MAPT* mutation carriers. We found topologically overlapping patterns of WM alterations across DTI and NODDI metrics in all *MAPT* mutation carriers, where regions showing the most robust statistical differences again involved frontotemporal areas and associated tracts. This suggests that both traditional DTI and NODDI measure

similar disease-related processes involved in the disruption of WM integrity. One crucial finding is the observation of widespread ODI patterns in asymptomatic carriers involving temporal and occipital WM as well as the superior and inferior fronto-occipital fasciculi, the cingulum, and the anterior limb of the internal capsule. In contrast, FA and MD revealed patterns of abnormalities restricted to temporal areas. This suggests that DTI and NODDI may have different sensitivities to WM abnormalities at different stages of the disease, and that ODI may be more sensitive than traditional DTI metrics to early WM changes in FTL. This would be in line with a handful of studies that have suggested biologically meaningful relationships between NODDI and measures of pathology in neurodegenerative diseases. For instance, two studies have found better sensitivity of ODI compared to FA and MD to histological measures of orientation dispersion in the spinal cord in amyotrophic lateral sclerosis patients (Grussu et al., 2015, 2017), and another recent study observed strong associations between NODDI metrics and in vivo imaging proxies and post-mortem measurements of tau and TDP-43 pathologies (Raghavan et al., 2022). While these studies did not specifically focus on asymptomatic carriers, they suggest that NODDI may have high sensitivity to biological disease-related changes in FTLs.

Another finding worth discussing is the discrepancy between tNDI and ODI findings in asymptomatic *MAPT* carriers, where widespread differences in ODI values were observed while lower tNDI values were only found in the amygdala. While the interpretation of this result remains highly speculative given the scarcity of published data on this topic, it is possible that ODI abnormalities reflect biological processes occurring in the earlier phase of the disease such as neuroinflammation (Sone et al., 2020) or dendritic arborization modifications (e.g., loosening or loss of complexity) as supported by findings in human (Broad et al., 2019) and animal models in amyotrophic lateral sclerosis (Fogarty et al., 2016; Jara et al., 2012). On the other hand, NDI may reflect neuronal and neurite loss, which typically occurs later in the disease course (Broad et al., 2019; Raghavan et al., 2021) (Broad et al., 2019; Raghavan et al., 2021). Thus, the finding of lower tNDI in the amygdala may be explained early focal tau-related degeneration as supported by findings in animals (Cook et al., 2014) and human (Bocchetta et al., 2019), while widespread ODI abnormalities may reflect other biological processes such as those mentioned above. Additional support for this hypothesis is the finding of a better discriminative values of the tNDI meta-ROI compared to FA in distinguishing *MAPT* carriers (while including symptomatic carriers) from controls. These groups comparisons contrast with the finding of significant correlations between tNDI values and estimated disease progression across all ROIs, while only the model in the cingulum was significant for ODI. This would be in line with the hypothesis above stating that increased axonal dispersion may be an early feature in the disease process, while neurite density may decrease more progressively throughout the disease course, although this statement is pending replication in future studies designed to address this question.

While this study represents an early step in using NODDI to characterize WM alterations in *MAPT* mutation carriers, and especially in asymptomatic carriers, our results are promising and have implications for therapeutic endeavors. One recent large-scale study by Staffaroni et al. (Staffaroni et al., 2022) used disease progression models to identify neuroimaging markers deemed most useful to design endpoints in clinical trials in f-FTL. However, this study did not include dMRI measurements. The fact that both DTI and NODDI metrics, especially FA and tNDI, tracked with estimated disease progression and that ODI appears to be a sensitive marker of early WM changes in *MAPT* mutation carriers argues for the inclusion of such measures in global initiatives aimed at the prevention and treatment of FTL. The inclusion of such metrics in the development of disease progression models could facilitate the planning of clinical trials by optimizing enrollment, tailoring desired endpoints, and reducing the number of patients required to detect therapy-induced effects. This is crucial given that treatments are most likely to be successful if initiated prior to the onset of clinical

symptoms (Boeve et al., 2022) and the rarity of f-FTLD, which is a major obstacle for enrollment purposes.

Our findings must be interpreted in the light of some limitations. While our sample was deeply phenotyped and was scanned using an advanced dMRI protocol that was not available in all of the ALLFTD Consortium sites, it was relatively small. This is particularly true for symptomatic carriers group, which was only composed of five patients. Thus, although the statistical effects in this group behaved in the expected direction, caution is warranted in the interpretation of these results which are pending replication in larger cohorts. While we used the Combat algorithm to harmonize multi-site data, this algorithm has not been tested in small datasets such as in this study. It is thus difficult to gauge the extent of inter-individual variability that is attributable to this factor. However, it is of note that ComBat derives its corrections using all the participants at each site, and it thus not directly affected by the number of carriers. The design of this study was cross-sectional. These limitations prevented us from assessing more complex and longitudinal relationships between dMRI metrics and disease progression. For instance, the relationships between MD, tNDI (amygdala) and ODI (cingulum) and estimated disease progression, although significant, were seemingly driven by symptomatic carriers. However, the sample size limitation did not allow us to assess slope change as a function of clinical status. This also speaks to the low prevalence of *MAPT* mutation carriers in the general population (Moore et al., 2020). It is also important to note that estimated age to symptom onset is an inherently imperfect measure of disease progression. Indeed, there exists high between- and within-family variability across and even within FTLD-related genetic mutations (Domoto-Reilly et al., 2017; Manoochehri et al., 2023), which may be due to factors such as cognitive reserve (Premi et al., 2013, 2017) or incomplete penetrance in some families with *MAPT* mutations (Anfossi et al., 2011; Munoz et al., 2007; Van Herpen et al., 2003). Another aspect is the limited availability of NODDI, which is an emerging imaging technique that is solely used in research context at the moment. It is noteworthy that group differences between asymptomatic carriers and controls, albeit significant, did not survive after correcting for multiple comparisons. Many factors may be at fault for this, including the small sample size or the inclusion of controls who were, on average, older than asymptomatic carriers. While we used age as a covariate in our models to mitigate this concern, the inclusion of controls comparable in terms of age would have been optimal. Therefore, one must remain cautious in interpreting these findings. Finally, a methodological limitation pertains to the susceptibility distortion caused by signal pileup in the temporal horns, which could not be corrected. This may have limited the accuracy and localization of those regions during image processing.

In conclusion, our results indicate that traditional DTI and NODDI measurements may offer different sensitivities across clinical stages in *MAPT* mutation carriers, and that ODI may be particularly sensitive to early WM degeneration in the asymptomatic phase of the disease. Moreover, various dMRI metrics tracked with estimated disease progression, suggesting that they could prove useful to estimate where a given individual stands along the disease spectrum and the risk of phenoconversion. While this study represents an early effort to examine the contribution of NODDI to decipher WM changes in f-FTLD, our results highlight the promising role of this imaging technique to detect the earliest brain abnormalities in *MAPT* mutations and to potentially optimize clinical trials.

## Funding

The ALLFTD consortium is funded by the National Institute on Aging (NIA) and the National Institute of Neurological Diseases and Stroke (NINDS) (U19: AG063911). The former ARTFL and LEFTDS consortia received funding from the NIA, NINDS and National Center for Advancing Translational Science (U54 NS092089, U01 AG045390). This work has also been funded by a grant awarded to the Alzheimer's

disease Research Center (AG 62677). Samples from the National Centralized Repository for Alzheimer's Disease and Related Dementias (NCRAD), which receives government support under a cooperative agreement grant (U24 AG21886) awarded by the NIA, were used in this study.

## CRedit authorship contribution statement

**Fields Julie A.:** Writing – review & editing, Investigation. **Ramanan Vijay K.:** Writing – review & editing, Investigation, Funding acquisition. **Graff-Radford Neill:** Writing – review & editing, Methodology, Investigation, Funding acquisition. **Botha Hugo:** Writing – review & editing, Methodology, Investigation, Funding acquisition. **Knopman David S.:** Writing – review & editing, Methodology, Investigation, Funding acquisition. **Graff-Radford Jonathan:** Writing – review & editing, Investigation. **Savica Rodolfo:** Writing – review & editing, Investigation, Funding acquisition. **Forsberg Leah K.:** Writing – review & editing, Project administration, Methodology, Investigation, Funding acquisition. **Wszolek Zbigniew:** Writing – review & editing, Investigation, Funding acquisition. **Heuer Hilary W.:** Writing – review & editing, Methodology, Investigation, Funding acquisition. **Tosakulwong Nirubol:** Writing – review & editing, Visualization, Methodology, Formal analysis, Data curation. **Petersen Ronald C.:** Writing – review & editing, Project administration, Investigation, Funding acquisition. **Corriveau-Lecavalier Nick:** Writing – original draft, Visualization, Project administration, Methodology, Formal analysis, Conceptualization. **Jack Clifford R.:** Writing – review & editing, Methodology, Investigation, Funding acquisition, Conceptualization. **Senjem Matthew L.:** Writing – review & editing, Methodology, Data curation. **Vemuri Prashanthi:** Writing – review & editing, Methodology, Investigation, Funding acquisition. **Jones David T.:** Writing – review & editing, Supervision, Investigation. **Rosen Howard J.:** Writing – review & editing, Resources, Methodology, Investigation, Funding acquisition. **Fought Angela J.:** Writing – review & editing, Visualization, Methodology, Formal analysis, Data curation. **Boxer Adam L.:** Writing – review & editing, Resources, Methodology, Investigation, Funding acquisition. **Lesnick Timothy G.:** Writing – review & editing, Visualization, Methodology, Formal analysis, Data curation. **Kantarci Kejal:** Writing – review & editing, Supervision, Resources, Project administration, Methodology, Investigation, Funding acquisition, Formal analysis, Conceptualization. **Schwarz Christopher G.:** Writing – review & editing, Methodology, Data curation. **Boeve Bradley F.:** Writing – review & editing, Supervision, Project administration, Methodology, Investigation, Funding acquisition, Conceptualization. **Reid Robert I.:** Writing – review & editing, Software, Methodology, Formal analysis, Data curation. **Rademakers Rosa:** Writing – review & editing, Investigation, Funding acquisition. **Geschwind Daniel H.:** Writing – review & editing, Methodology, Investigation, Funding acquisition. **Ramos Eliana Marisa:** Writing – review & editing, Methodology, Investigation, Funding acquisition, Data curation.

## Declaration of Competing Interest

CRJ receives no personal compensation from any commercial entity. He receives research support from National Institute of Health (NIH), the GHR Foundation, and the Alexander Family Alzheimer's Disease Research Professorship of the Mayo Clinic. RCP consults for Roche, Inc., Merck, Inc., Biogen, Inc., Genentech, Inc., Eisai, Inc., and Nestle, Inc. but does not receive significant fees due to NIH limitations from the U24 AG057437 Co-PI role. BB receives honoraria for SAB activities for the Tau Consortium, and has received research grant support but no personal compensation for clinical trials from Alector, Biogen, Transposon, Cognition Therapeutics, GE Healthcare. VKR receives research funding from the NIH and the Mangurian Foundation for Lewy Body disease research, has provided educational content for Medscape, is co-PI for a clinical trial supported by the Alzheimer's Association, and is a site

clinician for clinical trials supported by Eisai, the Alzheimer's Treatment and Research Institute at USC, and Transposon Therapeutics, Inc. EMR has no disclosure and receives funding from the NIH. ZKW is partially supported by the NIH/NIA and NIH/NINDS (1U19AG063911, FAIN: U19AG063911), Mayo Clinic Center for Regenerative Medicine, the gifts from the Donald G. and Jodi P. Heeringa Family, the Haworth Family Professorship in Neurodegenerative Diseases fund, and The Albertson Parkinson's Research Foundation. He serves as PI or Co-PI on Biohaven Pharmaceuticals, Inc. (BHV4157–206) and Vigil Neuroscience, Inc. (VGL101–01.002, VGL101–01.201, PET tracer development protocol, Csf1r biomarker and repository project, and ultra-high field MRI in the diagnosis and management of CSF1R-related adult-onset leukoencephalopathy with axonal spheroids and pigmented glia) projects/grants. He serves as Co-PI of the Mayo Clinic APDA Center for Advanced Research and as an external advisory board member for the Vigil Neuroscience, Inc., and as a consultant on neurodegenerative medical research for Eli Lilly & Company. KK consults Biogen, Inc.; receives research support from Avid Radiopharmaceuticals and Eli Lilly and receives funding from NIH and Alzheimer's Drug Discovery Foundation.

## Acknowledgments

We wish to express our gratitude towards all ALLFTD participants and their caregivers for the dedicated participation in this research program. We also thank all personnel involved in the ALLFTD consortium who are not listed as co-authors.

## Appendix A. Supporting information

Supplementary data associated with this article can be found in the online version at [doi:10.1016/j.neurobiolaging.2023.12.001](https://doi.org/10.1016/j.neurobiolaging.2023.12.001).

## References

- Andersson, J.L.R., Sotiropoulos, S.N., 2016. An integrated approach to correction for off-resonance effects and subject movement in diffusion MR imaging. *Neuroimage* 125, 1063–1078.
- Andersson, J.L.R., Graham, M.S., Zsoldos, E., Sotiropoulos, S.N., 2016. Incorporating outlier detection and replacement into a non-parametric framework for movement and distortion correction of diffusion MR images. *Neuroimage* 141, 556–572.
- Andersson, J.L.R., Graham, M.S., Drobnyak, I., Zhang, H., Filippini, N., Bastiani, M., 2017. Towards a comprehensive framework for movement and distortion correction of diffusion MR images: Within volume movement. *Neuroimage* 152, 450–466.
- Anfossi, M., Bernardi, L., Gallo, M., Geracitano, S., Colao, R., Puccio, G., Curcio, S.A.M., Frangipane, F., Mirabelli, M., Tomaino, C., 2011. MAPT V363I variation in a sporadic case of frontotemporal dementia: variable penetrant mutation or rare polymorphism? *Alzheimer Dis. Assoc. Disord.* 25 (1), 96–99.
- Avants, B.B., Tustison, N.J., Stauffer, M., Song, G., Wu, B., Gee, J.C., 2014. The Insight Toolkit image registration framework. *Frontiers in Neuroinformatics* 8, 44.
- Barker, M.S., Gottesman, R.T., Manoochehri, M., Chapman, S., Appleby, B.S., Brushaber, D., Devick, K.L., Dickerson, B.C., Domoto-Reilly, K., Fields, J.A., Forsberg, L.K., Galasko, D.R., Ghoshal, N., Goldman, J., Graff-Radford, N.R., Grossman, M., Heuer, H.W., Hsiung, G.Y., Knopman, D.S., Huey, E.D., 2022. Proposed research criteria for prodromal behavioural variant frontotemporal dementia. *Brain* 145 (3), 1079–1097. <https://doi.org/10.1093/brain/awab365>.
- Barritt, A.W., Gabel, M.C., Cercignani, M., Leigh, P.N., 2018. Emerging magnetic resonance imaging techniques and analysis methods in amyotrophic lateral sclerosis. *Front. Neurol.* 9, 1065.
- Bocchetta, M., Iglesias, J.E., Cash, D.M., Warren, J.D., Rohrer, J.D., 2019. Amygdala subnuclei are differentially affected in the different genetic and pathological forms of frontotemporal dementia. *Alzheimer's Dement.: Diagn., Assess. Dis. Monit.* 11, 136–141.
- Boeve, B.F., Boxer, A.L., Kumfor, F., Pijnenburg, Y., Rohrer, J.D., 2022. Advances and controversies in frontotemporal dementia: diagnosis, biomarkers, and therapeutic considerations. *Lancet Neurol.* 21 (3), 258–272.
- Broad, R.J., Gabel, M.C., Dowell, N.G., Schwartzman, D.J., Seth, A.K., Zhang, H., Alexander, D.C., Cercignani, M., Leigh, P.N., 2019. Neurite orientation and dispersion density imaging (NODDI) detects cortical and corticospinal tract degeneration in ALS. *J. Neurol., Neurosurg. Psychiatry* 90 (4), 404–411.
- Caruyer, E., Lenglet, C., Sapiro, G., Deriche, R., 2013. Design of multishell sampling schemes with uniform coverage in diffusion MRI. *Magn. Reson. Med.* 69 (6), 1534–1540.
- Cash, D.M., Bocchetta, M., Thomas, D.L., Dick, K.M., van Swieten, J.C., Borroni, B., Galimberti, D., Masellis, M., Tartaglia, M.C., Rowe, J.B., 2018. Patterns of gray matter atrophy in genetic frontotemporal dementia: results from the GENFI study. *Neurobiol. Aging* 62, 191–196.
- Chen, Q., Kantarci, K., 2020. Imaging biomarkers for neurodegeneration in presymptomatic familial frontotemporal lobar degeneration. *Front. Neurol.* 11, 80.
- Chen, Q., Boeve, B.F., Schwarz, C.G., Reid, R., Tosakulwong, N., Lesnick, T.G., Bove, J., Brannely, P., Brushaber, D., Coppola, G., 2019. Tracking white matter degeneration in asymptomatic and symptomatic MAPT mutation carriers. *Neurobiol. Aging* 83, 54–62.
- Chu, S.A., Flagan, T.M., Staffaroni, A.M., Jiskoot, L.C., Deng, J., Spina, S., Zhang, L., Sturm, V.E., Yokoyama, J.S., Seelye, W.W., 2021. Brain volumetric deficits in MAPT mutation carriers: a multisite study. *Ann. Clin. Transl. Neurol.* 8 (1), 95–110.
- Colgan, N., Siow, B., O'Callaghan, J.M., Harrison, I.F., Wells, J.A., Holmes, H.E., Ismail, O., Richardson, S., Alexander, D.C., Collins, E.C., 2016. Application of neurite orientation dispersion and density imaging (NODDI) to a tau pathology model of Alzheimer's disease. *Neuroimage* 125, 739–744.
- Cook, C., Dunmore, J.H., Murray, M.E., Scheffel, K., Shukoor, N., Tong, J., Castanedes-Casey, M., Phillips, V., Rousseau, L., Penular, M.S., 2014. Severe amygdala dysfunction in a MAPT transgenic mouse model of frontotemporal dementia. *Neurobiol. Aging* 35 (7), 1769–1777.
- Domoto-Reilly, K., Davis, M.Y., Keene, C.D., Bird, T.D., 2017. Unusually long duration and delayed penetrance in a family with FTD and mutation in MAPT (V337M). *Am. J. Med. Genet. Part B: Neuropsychiatr. Genet.* 174 (1), 70–74.
- Dopper, E.G.P., Rombouts, S.A.R.B., Jiskoot, L.C., Heijer, T., Den, De Graaf, J.R.A., De Koning, I., Hammerschlag, A.R., Seelaar, H., Seeley, W.W., Veer, I.M., Van Buchem, M.A., Rizzu, P., Van Swieten, J.C., 2014. Structural and functional brain connectivity in presymptomatic familial frontotemporal dementia. *Neurology* 83 (2). <https://doi.org/10.1212/WNL.0000000000000583>.
- Edwards, L.J., Pine, K.J., Ellerbrock, L., Weiskopf, N., Mohammadi, S., 2017. NODDI-DTI: estimating neurite orientation and dispersion parameters from a diffusion tensor in healthy white matter. *Front. Neurosci.* 11, 720.
- Fogarty, M.J., Klenowski, P.M., Lee, J.D., Drieberg-Thompson, J.R., Bartlett, S.E., Ngo, S.T., Hilliard, M.A., Bellingham, M.C., Noakes, P.G., 2016. Cortical synaptic and dendritic spine abnormalities in a presymptomatic TDP-43 model of amyotrophic lateral sclerosis. *Sci. Rep.* 6 (1), 37968.
- Fortin, J.-P., Parker, D., Tunç, B., Watanabe, T., Elliott, M.A., Ruparel, K., Roalf, D.R., Satterthwaite, T.D., Gur, R.C., Gur, R.E., 2017. Harmonization of multi-site diffusion tensor imaging data. *Neuroimage* 161, 149–170.
- Fumagalli, G.G., Basilico, P., Arighi, A., Bocchetta, M., Dick, K.M., Cash, D.M., Harding, S., Mercurio, M., Fenoglio, C., Pietrobboni, A.M., 2018. Distinct patterns of brain atrophy in Genetic Frontotemporal Dementia Initiative (GENFI) cohort revealed by visual rating scales. *Alzheimer's Res. Ther.* 10 (1), 1–9.
- Garyfalidis, E., Brett, M., Amirbekian, B., Rokem, A., Van Der Walt, S., Descoteaux, M., Nimmo-Smith, I., Contributors, D., 2014. Dipy, a library for the analysis of diffusion MRI data. *Front. Neuroinformatics* 8, 8.
- Grusso, F., Schneider, T., Zhang, H., Alexander, D.C., Wheeler-Kingshott, C.A.M., 2015. Neurite orientation dispersion and density imaging of the healthy cervical spinal cord in vivo. *Neuroimage* 111, 590–601.
- Grusso, F., Schneider, T., Tur, C., Yates, R.L., Tachrount, M., Ianuş, A., Yiannakas, M.C., Newcombe, J., Zhang, H., Alexander, D.C., 2017. Neurite dispersion: a new marker of multiple sclerosis spinal cord pathology? *Ann. Clin. Transl. Neurol.* 4 (9), 663–679.
- Jara, J.H., Villa, S.R., Khan, N.A., Bohn, M.C., Özdinler, P.H., 2012. AA2 mediated retrograde transduction of corticospinal neurons reveals initial and selective apical dendrite degeneration in ALS. *Neurobiol. Dis.* 47 (2), 174–183.
- Jiskoot, L.C., Bocchetta, M., Nicholas, J.M., Cash, D.M., Thomas, D., Modat, M., Ourselin, S., Rombouts, S.A.R.B., Dopper, E.G.P., Meeter, L.H., 2018. Presymptomatic white matter integrity loss in familial frontotemporal dementia in the GENFI cohort: A cross-sectional diffusion tensor imaging study. *Ann. Clin. Transl. Neurol.* 5 (9), 1025–1036.
- Jiskoot, L.C., Panman, J.L., Meeter, L.H., Dopper, E.G.P., Donker Kaat, L., Franzen, S., van der Ende, E.L., van Minkelen, R., Rombouts, S.A.R.B., Papma, J.M., 2019. Longitudinal multimodal MRI as prognostic and diagnostic biomarker in presymptomatic familial frontotemporal dementia. *Brain* 142 (1), 193–208.
- Kellner, E., Dhital, B., Kiselev, V.G., Reiser, M., 2016. Gibbs-ringing artifact removal based on local subvoxel-shifts. *Magn. Reson. Med.* 76 (5), 1574–1581.
- Knopman, D.S., Kramer, J.H., Boeve, B.F., Caselli, R.J., Graff-Radford, N.R., Mendez, M.F., Miller, B.L., Mercaldo, N., 2008. Development of methodology for conducting clinical trials in frontotemporal lobar degeneration. *Brain* 131 (11), 2957–2968.
- Koay, C.G., Özarslan, E., Basser, P.J., 2009. A signal transformational framework for breaking the noise floor and its applications in MRI. *J. Magn. Reson.* 197 (2), 108–119.
- Manoochehri, M., Huey, E.D., Rademakers, R., & Goldman, J. (2023). *Case report: TMEM106B haplotype alters penetrance of GRN mutation in frontotemporal dementia family.* 70(10), 1–5. <https://doi.org/10.3389/fneur.2023.1160248>.
- McKhann, G.M., Knopman, D.S., Chertkow, H., Hyman, B.T., Jack, C.R., Kawas, C.H., Klunk, W.E., Koroshetz, W.J., Manly, J.J., Mayeux, R., Mohs, R.C., Morris, J.C., Rossor, M.N., Scheltens, P., Carrillo, M.C., Thies, B., Weintraub, S., Phelps, C.H., 2011. The diagnosis of dementia due to Alzheimer's disease: Recommendations from the National Institute on Aging-Alzheimer's Association workgroups on diagnostic guidelines for Alzheimer's disease. *Alzheimer's Dement.* 7 (3), 263–269. <https://doi.org/10.1016/j.jalz.2011.03.005>.
- Moore, K.M., Nicholas, J., Grossman, M., McMillan, C.T., Irwin, D.J., Massimo, L., Van Deerlin, V.M., Warren, J.D., Fox, N.C., Rossor, M.N., 2020. Age at symptom onset and death and disease duration in genetic frontotemporal dementia: an international retrospective cohort study. *Lancet Neurol.* 19 (2), 145–156.
- Munoz, D.G., Ros, R., Fatas, M., Bermejo, F., de Yébenes, J.G., 2007. Progressive nonfluent aphasia associated with a new mutation V363I in tau gene. *Am. J. Alzheimer's Dis. Other Dementias* 22 (4), 294–299.

- Nasreddine, Z.S., Phillips, N.A., Bédirian, V., Charbonneau, S., Whitehead, V., Collin, I., Cummings, J.L., Chertkow, H., 2005. The Montreal Cognitive Assessment, MoCA: a brief screening tool for mild cognitive impairment. *J. Am. Geriatr. Soc.* 53 (4), 695–699.
- Oishi, K., Faria, A., Jiang, H., Li, X., Akhter, K., Zhang, J., Hsu, J.T., Miller, M.I., van Zijl, P.C.M., Albert, M., 2009. Atlas-based whole brain white matter analysis using large deformation diffeomorphic metric mapping: application to normal elderly and Alzheimer's disease participants. *Neuroimage* 46 (2), 486–499.
- Panman, J.L., Jiskoot, L.C., Bouts, M.J.R.J., Meeter, L.H.H., van der Ende, E.L., Poos, J. M., Feis, R.A., Kievit, A.J.A., Van Minkelen, R., Dopper, E.G.P., 2019. Gray and white matter changes in presymptomatic genetic frontotemporal dementia: a longitudinal MRI study. *Neurobiol. Aging* 76, 115–124.
- Peet, B.T., Spina, S., Mundada, N., La Joie, R., 2021. Neuroimaging in frontotemporal dementia: heterogeneity and relationships with underlying neuropathology. *Neurotherapeutics* 18, 728–752.
- Premi, E., Gazzina, S., Bozzali, M., Archetti, S., Alberici, A., Cercignani, M., Bianchetti, A., Gasparotti, R., Turla, M., Caltagirone, C., 2013. Cognitive reserve in granulin-related frontotemporal dementia: from preclinical to clinical stages. *PLoS One* 8 (9), e74762.
- Premi, E., Grassi, M., van Swieten, J., Galimberti, D., Graff, C., Masellis, M., Tartaglia, C., Tagliavini, F., Rowe, J.B., Laforce Jr, R., 2017. Cognitive reserve and TMEM106B genotype modulate brain damage in presymptomatic frontotemporal dementia: a GENFI study. *Brain* 140 (6), 1784–1791.
- Raghavan, S., Reid, R.I., Przybelski, S.A., Lesnick, T.G., Graff-Radford, J., Schwarz, C.G., Knopman, D.S., Mielke, M.M., Machulda, M.M., Petersen, R.C., 2021. Diffusion models reveal white matter microstructural changes with ageing, pathology and cognition. *Brain Commun.* 3 (2), fcab106.
- Raghavan, S., Przybelski, S.A., Reid, R.I., Lesnick, T.G., Ramanan, V.K., Botha, H., Matchett, B.J., Murray, M.E., Reichard, R.R., Knopman, D.S., 2022. White matter damage due to vascular, tau, and TDP-43 pathologies and its relevance to cognition. *Acta Neuropathol. Commun.* 10 (1), 16.
- Ramos, E.M., Dokuru, D.R., Van Berlo, V., Wojta, K., Wang, Q., Huang, A.Y., Deverasetty, S., Qin, Y., van Blitterswijk, M., Jackson, J., 2020. Genetic screening of a large series of North American sporadic and familial frontotemporal dementia cases. *Alzheimer's Dement.* 16 (1), 118–130.
- Rascovsky, K., Hodges, J.R., Knopman, D., Mendez, M.F., Kramer, J.H., Neuhaus, J., Van Swieten, J.C., Seelaar, H., Dopper, E.G.P., Onyike, C.U., Hillis, A.E., Josephs, K.A., Boeve, B.F., Kertesz, A., Seeley, W.W., Rankin, K.P., Johnson, J.K., Gorno-Tempini, M.L., Rosen, H., Miller, B.L., 2011. Sensitivity of revised diagnostic criteria for the behavioural variant of frontotemporal dementia. *Brain* 134 (9), 2456–2477. <https://doi.org/10.1093/brain/awr179>.
- Reid, R.I., Nedelska, Z., Schwarz, C.G., Ward, C., Jack, C.R., Initiative, A.D.N., 2018. Diffusion specific segmentation: skull stripping with diffusion MRI data alone. In *Computational Diffusion MRI*. Springer, pp. 67–80.
- Rohrer, J.D., Ridgway, G.R., Modat, M., Ourselin, S., Mead, S., Fox, N.C., Rossor, M.N., Warren, J.D., 2010. Distinct profiles of brain atrophy in frontotemporal lobar degeneration caused by progranulin and tau mutations. *Neuroimage* 53 (3), 1070–1076.
- Sieben, A., Van Langenhove, T., Engelborghs, S., Martin, J.-J., Boon, P., Cras, P., De Deyn, P.-P., Santens, P., Van Broeckhoven, C., Cruts, M., 2012. The genetics and neuropathology of frontotemporal lobar degeneration. *Acta Neuropathol.* 124, 353–372.
- Soares, J.M., Marques, P., Alves, V., Sousa, N., 2013. A hitchhiker's guide to diffusion tensor imaging. *Front. Neurosci.* 7, 31.
- Sone, D., Shigemoto, Y., Ogawa, M., Maikusa, N., Okita, K., Takano, H., Kato, K., Sato, N., Matsuda, H., 2020. Association between neurite metrics and tau/inflammatory pathology in Alzheimer's disease. *Alzheimer's & Dementia: Diagnosis Assess. Dis. Monit.* 12 (1), e12125.
- Staffaroni, A.M., Quintana, M., Wendelberger, B., Heuer, H.W., Russell, L.L., Cobigo, Y., Wolf, A., Goh, S.-Y.M., Petrucci, L., Gendron, T.F., 2022. Temporal order of clinical and biomarker changes in familial frontotemporal dementia. *Nat. Med.* 28 (10), 2194–2206.
- Thomason, M.E., Thompson, P.M., 2011. Diffusion imaging, white matter, and psychopathology. *Annu. Rev. Clin. Psychol.* 7, 63–85.
- Van Herpen, E., Rosso, S.M., Serverijnen, L., Yoshida, H., Breedveld, G., Van De Graaf, R., Kamphorst, W., Ravid, R., Willemsen, R., Dooijes, D., 2003. Variable phenotypic expression and extensive tau pathology in two families with the novel tau mutation L315R. *Ann. Neurol.: Off. J. Am. Neurol. Assoc. Child Neurol. Soc.* 54 (5), 573–581.
- Veraart, J., Fieremans, E., Novikov, D.S., 2016. Diffusion MRI noise mapping using random matrix theory. *Magn. Reson. Med.* 76 (5), 1582–1593.
- Whitwell, J.L., Jack, C.R., Boeve, B.F., Senjem, M.L., Baker, M., Rademakers, R., Ivnik, R. J., Knopman, D.S., Wszolek, Z.K., Petersen, R.C., 2009. Voxel-based morphometry patterns of atrophy in FTL with mutations in MAPT or PGRN. *Neurology* 72 (9), 813–820.
- Zhang, H., Schneider, T., Wheeler-Kingshott, C.A., Alexander, D.C., 2012. NODDI: practical in vivo neurite orientation dispersion and density imaging of the human brain. *Neuroimage* 61 (4), 1000–1016.